RSC Advances

ROYAL SOCIETY OF CHEMISTRY

www.rsc.org/advances

RSC Advances

ARTICLE

Efficient hydrogen generation from formic acid using AgPd nanoparticles immobilized on carbon nitride-functionalized SBA-15

Received 00th January 20xx,
Accepted 00th January 20xx

DOI: 10.1039/x0xx00000x

www.rsc.org/

Lixin Xu[a], Bo Jin[a], Jian Zhang[a], Dang-guo Cheng[b], Fengqiu Chen[b], Yue An[b], Ping Cui [a], and Chao Wan[a,*]

Bimetallic AgPd nanoparticles were successfully immobilized on graphitic carbon nitride (g-C_3N_4) functionalized SBA-15 for the first time by a facile co-reduction method. These catalysts were applied in the decomposition of formic acid. The dehydrogenation of formic acid is dependent on the composition of AgPd and the content of carbon nitride (CN). Among all of the AgPd/mCND/SBA-15 catalysts tested, the $Ag_{10}Pd_{90}$/0.2CND/SBA-15 catalyst exhibits exceedingly superior performance for the decomposition of formic acid into high-quality hydrogen at 323 K with 100% hydrogen selectivity and a turnover frequency of 893 h^{-1}, which is among the maximum values obtained at 323 K in this paper. The improved performance is a promising step towards the utilization of formic acid as a hydrogen storage material.

1. Introduction

Considering the current energy crisis, where the consumption of fossil fuels and consequent environmental pollution increase continuously, it is highly desirable to search for renewable, benign, and sustainable energy sources. Among a variety of alternative energy, hydrogen, generating only water as a byproduct, has been proposed as an environmentally attractive, clean, and efficient energy carrier for its extensive utilization in proton exchange membrane fuel cells.[1,2] However, searching for efficient and safe hydrogen storage materials is one of the most critical challenges that hinders the development of hydrogen energy.[3-6] Formic acid (FA, HCOOH), a natural biomass accessible *via* CO_2 reduction, has attracted much attention due to its excellent stability, high energy density, and non-toxicity.[7-12] FA can decompose through two principal routes, dehydrogenation (eq. (1)) and dehydration (eq. (2)). The former produces hydrogen (H_2) and carbon dioxide (CO_2) while the latter produces water (H_2O) and carbon monoxide (CO), which is highly toxic to catalysts.[13-16] Therefore, it is highly desirable to develop efficient and cost-effective catalysts for the decomposition of FA.

HCOOH (l) = CO_2 (g) + H_2 (g) $\Delta G = -35.0$ kJ mol^{-1} (1)

HCOOH (l) = CO (g) + H_2O (g) $\Delta G = -14.9$ kJ mol^{-1} (2)

In recent years, the decomposition of FA has been investigated using various homogeneous Fe,[17] Ir,[18] and Ru[19,20] catalysts, as well as a number of heterogeneous Pd and Au noble metal catalysts.[10-12,21-24] Although some of these homogeneous catalysts exhibit high activities and selectivities for the decomposition of FA, their difficult recovery from the reaction mixture impedes their practical application.[25] Consequently, due to the ease of carrying and separation, much effort has been concentrated on the development of metal nanoparticles (NPs) with high activity and selectivity for the decomposition of FA.[26-30] To date, most work on NPs for FA dehydrogenation has been focused on bimetallic and trimetallic composites.[31-33] The performance of nanocatalysts is highly dependent on their particle size, crystallinity, dispersion, support, etc.[34-36]

Zhang *et al.*[37] reported a Schiff base (C=N) as an active group with broaden applications in a great deal of homogeneous processes, and metal–Schiff base complexes were also reported to display catalytic activity in numerous reactions such as Heck reactions,[38] hydrogenation,[39] and even the decomposition of FA.[40] In consequence, the functionalization of a Schiff base over supported metal nanocatalysts presents a promising route for designing catalysts for the dehydrogenation of FA, although heterogenization of a Schiff base over a support is challenging. In the approach used in this study, polymeric carbon nitrides (CN) are employed to functionalize SBA-15 supports to stabilize metal NPs. CN-modified SBA-15 was first impregnated with a layer of CN using dicyandiamide as a precursor before being used to support AgPd bimetallic NPs. These catalysts were then applied in the decomposition of FA/sodium formate (SF). X-ray diffraction (XRD), transmission electron microscopy (TEM), and X-ray photoelectron spectroscopy (XPS) were used for structural investigations. The generated gas was analyzed by a gas chromatograph connected to a thermal conductivity detector (TCD).

[a] College of Chemistry and Chemical Engineering, Anhui University of Technology, 59 Hudong Road, Ma'anshan 243002, China
[b] College of Chemical and Biological Engineering, Zhejiang University, 38 Zheda Road, Hangzhou 310027, China
E-mail:wanchao1219@hotmail.com
Electronic Supplementary Information (ESI) available.
See DOI: 10.1039/x0xx00000x

2. Experimental

2.1 Materials

Palladium(II) chloride ($PdCl_2$, AR, Sinopharm Chemical Reagent Co., Ltd.), silver nitrate ($AgNO_3$, AR, Sinopharm Chemical Reagent Co., Ltd.), FA (98%, Aladdin Industrial Inc.), hydrochloric acid (HCl, 37%, Sinopharm Chemical Reagent Co., Ltd.), tetraethyl orthosilicate (TEOS, Sinopharm Chemical Reagent Co., Ltd., AR), Pluronic P123 triblock copolymer ($EO_{20}PO_{70}EO_{20}$, M_{av} = 5800, Sigma-Aldrich), ethanol (C_2H_5OH, Sinopharm Chemical Reagent Co., Ltd., AR) sodium borohydride ($NaBH_4$, 96%, Sinopharm Chemical Reagent Co., Ltd.), dicyandiamide ($C_2H_4N_4$, 98%, Aladdin Industrial Inc.), potassium chloride (KCl, 99%, Sinopharm Chemical Reagent Co. Ltd.), and sodium formate (HCOONa, 99%, Sinopharm Chemical Reagent Co. Ltd.) were employed as-purchased. Deionized water with a conductance below 10^{-6} S/cm was used in all synthesis and washing processes.

2.2 Preparation of CND/SBA-15 materials

SBA-15 was prepared using Pluronic P123 triblock copolymer as a template according to the procedure reported by Zhao *et al*.[41] In a typical process, 2.0 g P123 was dissolved in 15.0 g water, followed by the addition of 60.0 g 2 M HCl aqueous solution. Next, 4.25 g TEOS was added into the mixture under stirring, and further stirred at 313 K for 24 h. The milky liquid was transferred into an autoclave and hydrothermally treated at 373 K for 24 h. Afterwards, the white precipitate was filtered and dried at 333 K overnight. The SBA-15 support was obtained by calcining at 823 K for 5 h to remove P123.

Dicyandiamide (DCDA, 0.1 g) was dissolved in ethanol/water (60/15 mL) by heating to 353 K and kept at this temperature for 10 min to guarantee the complete dissolution of DCDA. The above-mentioned dicyandiamide solution was added to the previously dried SBA-15 (1 g) solid. After 6 h digestion, the mixture was heated at 373 K until ethanol and water were evaporated to form a white solid. Next, the resultant solid was ground in a mortar, heated at 2.5 K min^{-1} up to 873 K under a N_2 atmosphere (flow rate: 40 mL min^{-1}), and then treated for a further 4 h.[42,43] The obtained sample was labeled as 0.1CND/SBA-15. Based on the dicyandiamide content, the products were denoted as mCND/SBA-15, where m represents the mass of DCDA (m = 0.2, 0.3, 0.4).

2.3 Synthesis of AgPd/mCND/SBA-15 catalysts

Potassium tetrachloropalladinic acid (0.06 M, K_2PdCl_4) solution was prepared by adding 1 g $PdCl_2$ to 100 mL KCl (0.84 g) aqueous solution at 298 K under stirring for complete dissolution.

Bimetallic AgPd/mCND/SBA-15 catalysts with various molar ratios of Ag/Pd were synthesized. In brief, for the preparation of $Ag_{10}Pd_{90}$/0.1CND/SBA-15, 0.1CND/SBA-15 (200 mg) was placed into a 20 mL mixture solution of $AgNO_3$ (0.04 mmol) and K_2PdCl_4 (0.36 mmol) at 298 K under stirring for 24 h to immobilize the two metal precursors onto the support. Next, the obtained mixture was reduced with fresh $NaBH_4$ aqueous solution (2 mmol) under vigorous stirring. Finally, the $Ag_{10}Pd_{90}$/0.1CND/SBA-15 catalyst was obtained by centrifugation, washed with deionized water and ethanol, and dried at 333 K for 12 h. For comparison, $Ag_{10}Pd_{90}$/0.2CND/SBA-15, $Ag_{10}Pd_{90}$/0.3CND/SBA-15, $Ag_{10}Pd_{90}$/0.4CND/SBA-15, Ag/0.2CND/SBA-15, Pd/0.2CND/SBA-15, $Ag_{20}Pd_{80}$/0.2CND/SBA-15, and $Ag_{30}Pd_{70}$/0.2CND/SBA-15 were prepared by the same method. (Scheme 1)

2.4 Hydrogen generation from FA aqueous solution

2.4.1 Hydrogen release from FA/SF over AgPd/mCND/SBA-15. Typically, as-prepared AgPd/mCND/SBA-15 (100 mg) was placed into a two-necked round-bottomed flask with one neck used for introducing a 2 mL mixture of FA (3 mmol) and SF (1 mmol), and the other for connection to a gas burette. The dehydrogenation reaction was initiated at the desired temperature once the FA/SF mixture solution was injected into the two-necked flask with magnetic stirring. The release of gas was measured by the gas burette. This reaction was performed at 323 K under ambient atmosphere. The catalytic performance of all catalysts for the dehydrogenation of FA was investigated by the above procedure.

2.4.2 NaOH trap test.

In order to measure the composition of H_2 and CO_2 in the gas mixture released during the AgPd/mCND/SBA-15-catalyzed decomposition of aqueous FA/SF solution, NaOH trap tests were conducted, according to a previously reported procedure.[35,36] In a typical procedure, the trap (10 M NaOH solution) was placed between the gas burette and reactor. The gas produced from the dehydrogenation reaction was measured by passing through the NaOH trap and comparing to that generated in experiments without a trap.

2.5 Characterization

The detailed composition of the catalysts was measured by inductively coupled plasma-atomic emission spectroscopy (ICP-AES, Thermo iCAP6300) and elementary analysis (PerkinElmer EA2400 II). Powder XRD patterns were acquired on a Bruker D8-Advance X-ray diffractometer with a velocity of 1^o min^{-1} using a Cu Kα radiation source (λ = 0.154178 nm). Surface area measurements were conducted using nitrogen adsorption/desorption isotherms at 77 K after dehydration under vacuum at 423 K for 8 h using a Micromeritics ASAP 2020 analyzer. XPS measurements were performed on a Thermo Scientific Escalab 250Xi with Al Kα radiation as the excitation source. TEM experiments were conducted on an FEI Tecnai F20 transmission electron microscope operating at 200 kV. Detailed gas analyses were conducted on a GC-9860 II (Shanghai Qiyang Information Technology Co., Ltd.) with a TCD for CO_2 and H_2, and a flame ionization detector (FID)-Methanator for CO (detection limit: ~10 ppm for CO).

3. Results and discussion

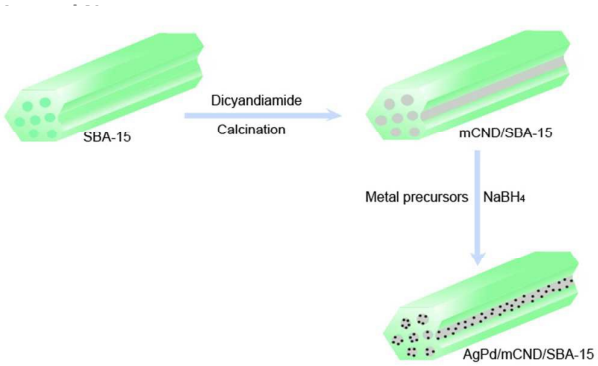

Scheme 1 Schematic illustration for the preparation of AgPd/mCND/SBA-15.

mCND/SBA-15 was prepared following a previously reported procedure.[42,43] As displayed in scheme 1, monodisperse AgPd/mCND/SBA-15 was synthesized by a one-step co-reduction method in 1 h at 273 K, and $AgNO_3$, K_2PdCl_4, and mCND/SBA-15 were added as the metal precursors, while $NaBH_4$ was used as the reducing agent. The composition of AgPd in AgPd/mCND/SBA-15 was modified by changing the designed molar ratio of $AgNO_3$ and K_2PdCl_4, and measured using ICP-AES, as displayed in Table S1. $Ag_{10}Pd_{90}$/0.2CND/SBA-15, $Ag_{20}Pd_{80}$/0.2CND/SBA-15, $Ag_{30}Pd_{70}$/0.2CND/SBA-15, Ag/0.2CND/SBA-15, and Pd/0.2CND/SBA-15 were prepared using metal precursors at Ag/Pd ratios of 1:9, 2:8, 3:7, 1:0, and 0:1, respectively. $Ag_{10}Pd_{90}$/mCND/SBA-15 catalysts with different CN content were also investigated. It should be noted that the dehydrogenation activity of the AgPd/mCND/SBA-15 catalysts for FA/SF was strongly dependent on Ag/Pd composition and CN content. As shown in Fig. 1 and Table S2, the initial turnover frequency ($TOF_{initial}$) reached the optimal value at an Ag molar ratio of 0.1; too little or too much Ag in the AgPd alloy can lead to a much lower activity. Based on the above

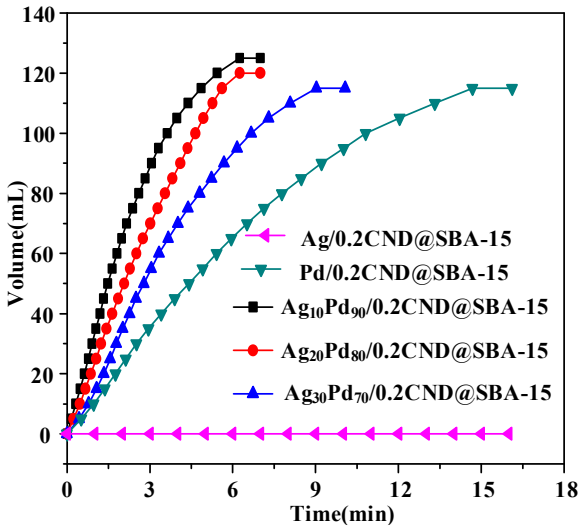

Fig. 1 Hydrogen generation from FA/SF with different of Ag/Pd content immobilized on 0.2CND/SBA-15 versus time at 323 K (n_{FA}=3 mmol, n_{SF}=1 mmol).

results, the $Ag_{10}Pd_{90}$/0.2CND/SBA-15 catalyst showed the best activity for the decomposition of FA/SF; the volume of released gas over 6.25 min reached 125 mL at 323 K. The $Ag_{10}Pd_{90}$/0.2CND/SBA-15 catalyst demonstrates superior activity with a TOF value of 893 h^{-1} at 323 K (Table 1), and 100% selectivity for hydrogen release from FA/SF. As shown in Fig. 2, the content of CN in $Ag_{10}Pd_{90}$/mCND/SBA-15 has a great influence on the dehydrogenation of FA/SF. Compared with $Ag_{10}Pd_{90}$/SBA-15, $TOF_{initial}$ over $Ag_{10}Pd_{90}$/mCND/SBA-15 shows a volcano plot with respect to CN content. $Ag_{10}Pd_{90}$/0.2CND/SBA-15 was clearly the optimal catalyst for dehydrogenation in this study.

Table. 1 Comparison performance of different catalysts for hydrogen released from FA/SF.

Catalyst	T (K)	TOF (h^{-1})	E_a (kJ/mol)	Reference
$Ag_{10}Pd_{90}$/0.2CND/SBA-15	323	893	43.2	This work
Au/C	323	80		15
Monodisperse $Ag_{42}Pd_{58}$/C	323	382	22	44
$Ni_{18}Ag_{24}Pd_{58}$/C	323	85	20.5	45
Pd/C	323	30		15
Monodisperse $Au_{41}Pd_{59}$/C	323	230	28	15
PdAu/C-CeO_2	365	113.5		46
AuPd@ED-MIL-101	363	106		47
Ag@Pd	293	125	30.0	48
Ag/Pd alloy	293	144	30	48

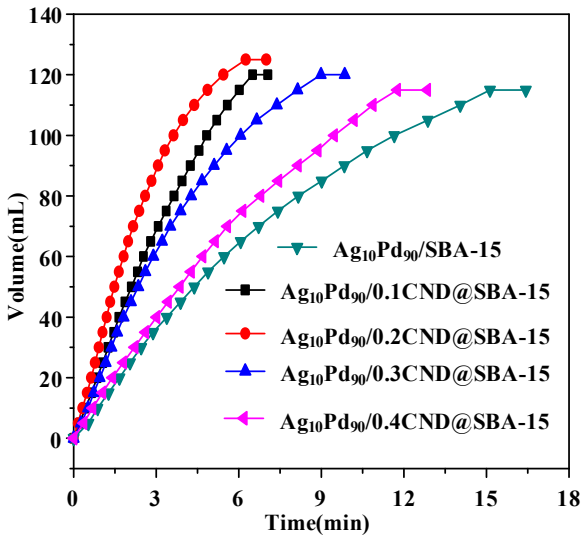

Fig. 2 Hydrogen generation from FA/SF over $Ag_{10}Pd_{90}$/mCND/SBA-15 with different of CN content versus time at 323 K (n_{FA}=3 mmol, n_{SF}=1 mmol).

In order to confirm the composition of released gas, the gas was passed through a 10 M NaOH solution trap, which can confirm complete absorption of CO_2 from the gas.[35,36,49,50] The volume of gas reduced to half the original value after passing through the NaOH trap, as shown in Fig. S1, implying that the dehydrogenation reaction generates only carbon dioxide and hydrogen without releasing CO. Furthermore, gas chromatography (GC) analyses further confirmed the presence of CO_2 and absence of CO, as shown in Fig. S2 and S3. Based on the above results, the $Ag_{10}Pd_{90}$/0.2CND/SBA-15 catalyst exhibited excellent H_2 selectivity for the decomposition of FA/SF.

The dehydrogenation reactions of FA/SF catalyzed by $Ag_{10}Pd_{90}$/0.2CND/SBA-15 were conducted at a series of temperatures in the range of 323–353 K in order to obtain the activation energy (E_a) of this reaction.[49-51] The values of the rate constant k at various temperatures can be acquired according to the slope of the linear part of each plot in Fig. 3a. The Arrhenius plot of ln$k$ *vs.* 1/T for this catalyst is revealed in Fig. 3b, from which the apparent activation energy could be calculated to be approximately 43.2 kJ mol^{-1} (Table 1). As displayed in Fig. S4, it can be observed that the catalytic activity of catalyst decrease obviously after the fourth run. It can be revealed in Fig.S5 that the reason for the decrease in their catalytic performance may be attributed to the increasing of the particle size, which is consistent with ths literature reported. [36]

The small XRD angles of the $Ag_{10}Pd_{90}$/mCND/SBA-15 catalysts with different CN content show similar diffraction peaks assignable to SBA-15 (Fig. 4), suggesting that the porous structure of SBA-15 remains unchanged irrespective of the formation of CN, in accordance with previous results.[42,43] Fig. 5a shows the N_2 adsorption/desorption isotherms of $Ag_{10}Pd_{90}$/ mCND/SBA-15. All samples demonstrate type IV isotherms

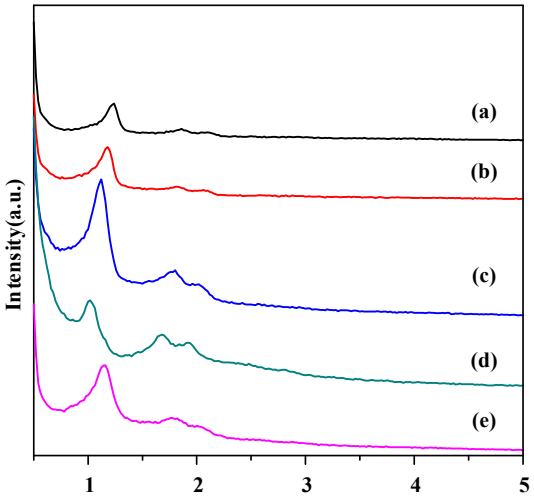

Fig. 4 Small-angle XRD patterns of all samples: (a) $Ag_{10}Pd_{90}$/SBA-15; (b) $Ag_{10}Pd_{90}$/0.1CND/SBA-15; (c) $Ag_{10}Pd_{90}$/0.2CND/SBA-15; (d) $Ag_{10}Pd_{90}$/0.3CND/SBA-15; (e) $Ag_{10}Pd_{90}$/0.4CND/SBA-15.

with H1-type hysteresis loops attributing to ordered mesoporous structures, implying that the pore structure of SBA-15 is not damaged after the generation of CN, in consistent with the XRD results shown in Fig. 4. As can be seen in Fig. 5b, the $Ag_{10}Pd_{90}$/mCND/SBA-15 catalysts contain one type of pore with small mesopores (the center of pore distribution from the adsorption branch is 8 nm).

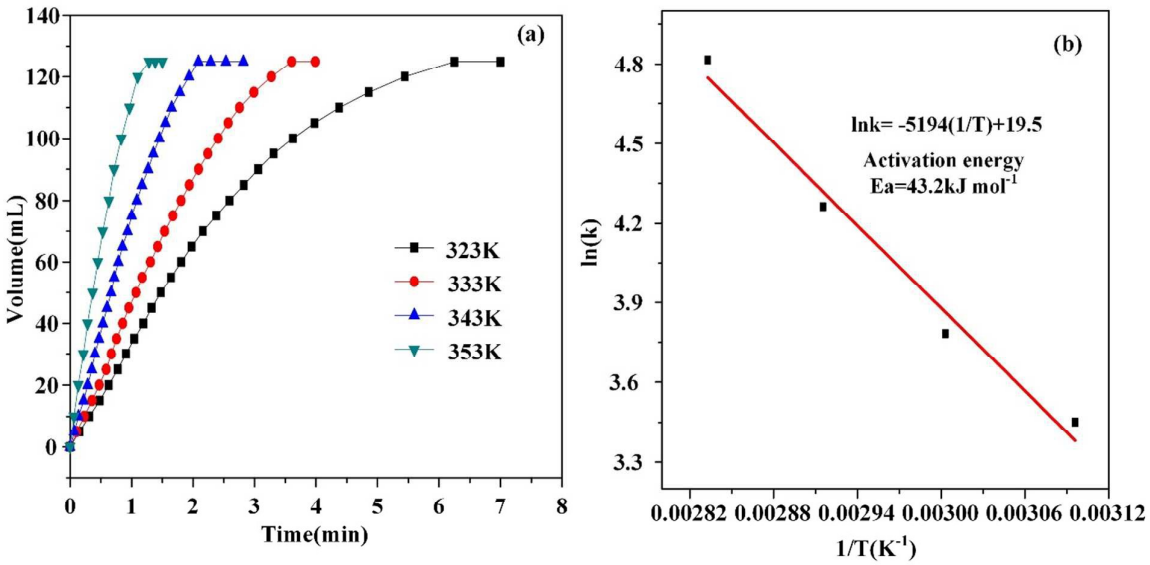

Fig. 3 (a) Time course plots for gas produced by the dehydrogenation of FA/SF by $Ag_{10}Pd_{90}$/0.2CND/SBA-15 at different temperatures. (b) Arrhenius plot of ln k *vs.* 1/T over $Ag_{10}Pd_{90}$/0.2CND/SBA-15 according to the data of (a) (n_{FA} = 3 mmol, n_{SF} = 1 mmol).

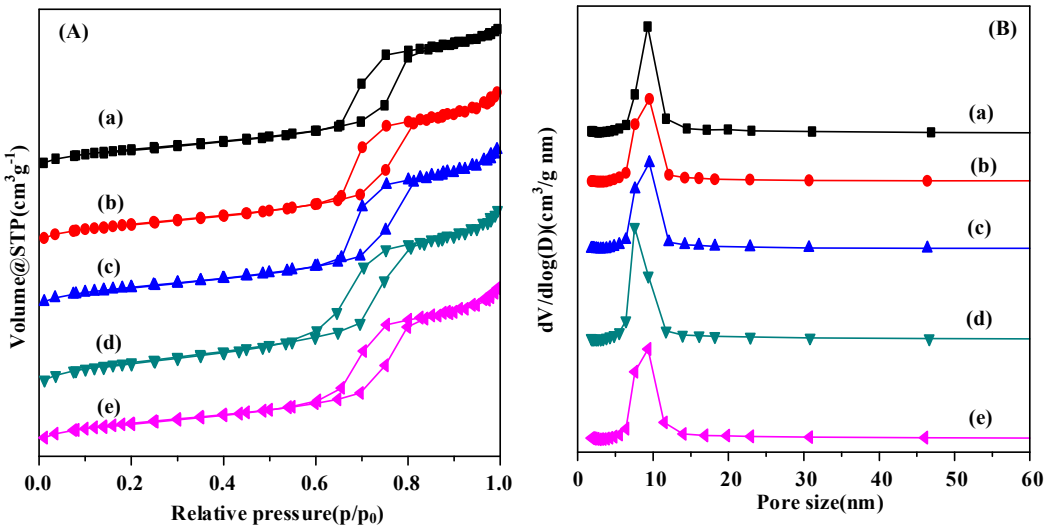

Fig. 5 Nitrogen adsorption–desorption isotherms (A) and pore size distributions (B) of all samples: (a) $Ag_{10}Pd_{90}$/SBA-15; (b) $Ag_{10}Pd_{90}$/0.1CND/SBA-15; (c) $Ag_{10}Pd_{90}$/0.2CND/SBA-15; (d) $Ag_{10}Pd_{90}$/0.3CND/SBA-15; (e) $Ag_{10}Pd_{90}$/0.4CND/SBA-15.

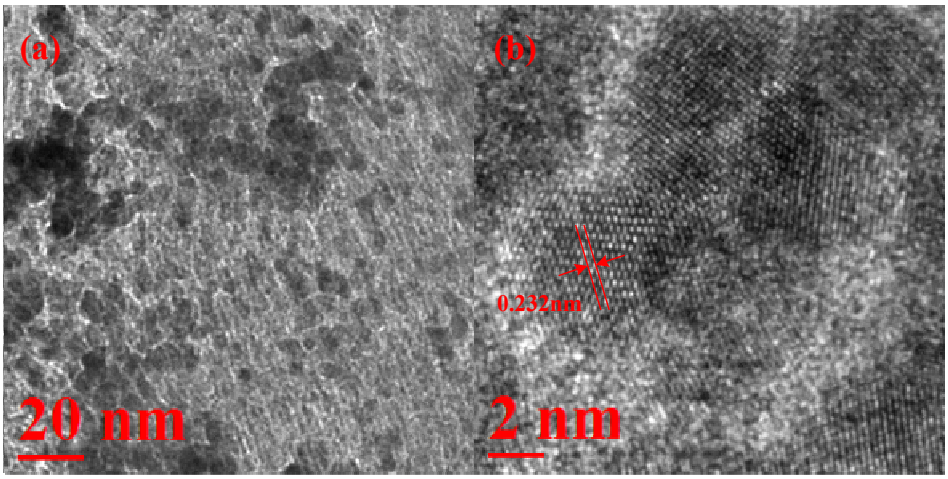

Fig. 6 (a-b) TEM images of $Ag_{10}Pd_{90}$/0.2CND/SBA-15 with different magnification.

The morphology of $Ag_{10}Pd_{90}$/0.2CND/SBA-15 was further characterized by TEM (Fig. 6). The TEM images of $Ag_{10}Pd_{90}$/0.2CND/SBA-15 demonstrate that the AgPd NPs are well dispersed in 0.2CND/SBA-15. The nitrogen content of Ag10Pd90/0.2CND/SBA-15 was 3.5wt%. The mean diameter of AgPd NPs in Ag10Pd90/0.2CND/SBA-15 was in the range of 4.5 ± 0.5 nm (Fig. S6), which is small enough for immobilization into the mesoporous cavities of 0.2CND/SBA-15 (8 nm). As revealed in Fig. 6b, the representative HRTEM image shows a d-spacing of 0.232 nm, which is between the (111) lattice spacing of face-centered cubic fcc Pd (0.22 nm) and (fcc) Ag (0.24 nm), further confirming that AgPd is existed as an alloy structure.[49-51] Fig. S7 display the related element mapping of Si, O, C, N, Ag and Pd of $Ag_{10}Pd_{90}$/0.2CND/SBA-15 and the high-angle annular dark field scanning TEM (HAADF-STEM), respectively. It can be observed that the elements of C, N, Ag and Pd have a similar distribution map. The results proved the hypothesis that we designed above about the preparation for the catalyst. In addition, the XRD patterns at 38.03° and 40.10° in Fig.S8 can be ascribed to Ag/0.2CND/SBA-15 and Pd/0.2CND/SBA-15, respectively. The XRD patterns of $Ag_{10}Pd_{90}$/0.2CND/SBA-15, $Ag_{20}Pd_{80}$/0.2CND/SBA-15 and $Ag_{30}Pd_{70}$/0.2CND/SBA-15 show a series of diffraction peaks that located between the diffraction patterns of pure Pd and Ag with a face-centered cubic structure, also suggesting the formation of AgPd alloy nanoparticles.[50,51]

XPS was conducted to investigate the chemical composition and elucidate the elemental chemical states of $Ag_{10}Pd_{90}$/0.2CND/SBA-15. Fig. 7 shows high-resolution XPS spectra of Ag (3d), Pd (3d), C (1s), and N (1s) observed in $Ag_{10}Pd_{90}$/0.2CND/SBA-15. The XPS results (Fig. 7) of $Ag_{10}Pd_{90}$/0.2CND/SBA-15 reveal the presence of metallic Ag^0, with Ag $3d_{5/2}$ at 367.5 eV and Ag $3d_{3/2}$ at 373.5 eV, as well as

metallic Pd^0, with Pd $3d_{5/2}$ at 335.3 eV and Pd $3d_{3/2}$ at 340.6 eV.[34,35,49-51] These binding energy shifts of the core electrons

AgPd/mCND/SBA-15 for the dehydrogenation of FA for the first time. The $Ag_{10}Pd_{90}$/0.2CND/SBA-15 catalyst demonstrated remarkably superior activity with $TOF_{initial}$ = 893 h^{-1} at 323 K. This newly designed

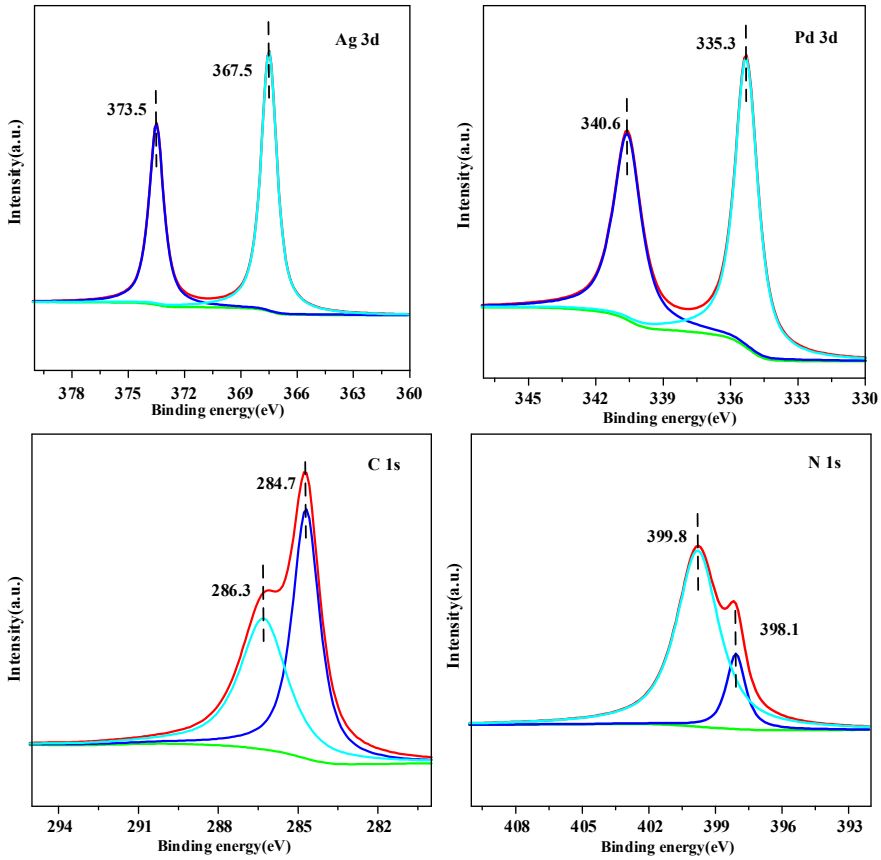

Fig. 7 XPS spectra of $Ag_{10}Pd_{90}$/0.2CND/SBA-15.

reveal that some electrons are changed, confirming the alloy structure of $Ag_{10}Pd_{90}$ NPs in $Ag_{10}Pd_{90}$/0.2CND/SBA-15, in accordance with previous reports.[49-51] The C 1s spectrum can be deconvoluted into two peaks at 286.3 and 284.7 eV, ascribed to the sp^2 C atoms bonded to N inside the aromatic structure and adventitious carbon impurities, respectively. Two peaks are observed in the N 1s spectrum of $Ag_{10}Pd_{90}$/0.2CND/SBA-15 at 399.8 and 398.1 eV, which can be attributed to pyrrolic or pyridonic N (C–N) and sp^2-hybridized nitrogen atoms involved in pyridinic N (C=N–C), respectively. These assignments are consistent with the reported data for CN.[52] More importantly, the presence of a Schiff base can drastically improve dehydrogenation performance, which is consistent with the results reported by Zhang *et al.*[37]

Conclusions

In summary, we successfully synthesized a highly efficient heterogeneous catalyst using AgPd alloy NPs deposited on g-C_3N_4-functionalized SBA-15, and applied it to the dehydrogenation of FA/SF. We also investigated the synergistic effect of $Ag_{10}Pd_{90}$/0.2CND/SBA-15 catalyst shows great potential as an efficient catalyst for the decomposition of FA, which is important for future applications of FA as a H_2 storage material.

Acknowledgements

Financial supports from National Natural Science Foundation of China (21376005, 21476001) and the Program for Zhejiang Leading Team of S&T Innovation (2013TD07) are gratefully appreciated.

Notes and references

1 J.M. Petersen, F.U. Zielinski, T. Pape, R. Seifert, C. Moraru, R. Amann, S. Hourdez, P. R. Girguis, S. D. Wankel, V. Barbe, E. Pelletier, D. Fink, C. Borowski, W. Bach and N. Dubilier, *Nature*, 2011, **476**, 176–180.
2 L. M. Amoo and R. L. Fagbenle, *Int. J Hydrogen Energy*, 2014, **39**, 12409–33.
3 J. Graetz, *Chem. Soc. Rev.*, 2009, **38**, 73–82.

4 Q. L. Zhu and Q. Xu, *Energy Environ. Sci.*, 2015, **8**, 478–512.
5 J. Yang, A. Sudik, C. Wolverton and D. J. Siegel, *Chem. Soc. Rev.*, 2010, **39**, 656–675.
6 U. Eberle, M. Felderhoff and F. Schuth, *Angew Chem. Int. Ed.*, 2009, **48**, 6608–6630.
7 A. K. Singh, S. Singh and A. Kumar, *Catal. Sci. Technol.*, 2016, **6**, 12–40.
8 S. Ott, *Science*, 2011, **333**, 1714–5.
9 L. J. Jia, D. A. Bulushev, O. Y. Podyacheva, A. I. Boronin, L. S. Kibis, E. Y. Gerasimov, S. Beloshapkin, I. A. Seryak, Z. R. Ismagilov and J. R. H. Ross, *J. Catal.*, 2013, **307**, 94–102.
10 X. J. Gu, Z. H. Lu, H. L. Jiang, T. Akita and Q. Xu, *J. Am. Chem. Soc.*, 2011, **133**, 11822–11825.
11 Q. L. Zhu, N. Tsumori and Q. Xu, *Chem. Sci.*, 2014, **5**, 195–199.
12 W. Y. Yu, G. M. Mullen, D. W. Flaherty and C. B. Mullins, *J. Am. Chem. Soc.*, 2014, **136**, 11070–11078.
13 F. Jóo, *ChemSusChem*, 2008, **1**, 805–808;
14 A. Boddien, D. Mellmann, F. Gärtner, R. Jackstell, H. Junge, P. J. Dyson, G. Laurenczy, R. Ludwig and M. Beller, *Science*, 2011, **333**, 1733–1736.
15 Ö. Metin, X. L. Sun and S. H. Sun, *Nanoscale*, 2013, **5**, 910–912.
16 C. Q. Hu, S. W. Ting, K. Y. Chan and W. Huang, *Int. J Hydrogen Energy*, 2013, **38**, 8720–8731.
17 E. A. Bielinski, P. O. Lagaditis, Y. Y. Zhang, B. Q. Mercado, C. Würtele, W. H. Bernskoetter, N. Hazari and S. Schneider, *J. Am. Chem. Soc.*, 2014, **136**, 10234−10237.
18 W. H. Wang, M. Z. Ertem, S. A. Xu, N. Onishi, Y. Manaka, Y. Suna, H. Kambayashi, J. T. Muckerman, E. Fujita and Y. Himeda, *ACS Catal.*, 2015, **5**, 5496−5504.
19 A. Thevenon, E. Frost-Pennington, G. Weijia, A. F. Dalebrook and G. Laurenczy, *ChemCatChem*, 2014, **6**, 3146−3152.
20 S. F. Hsu, S. Rommel, P. Eversfield, K. Muller, E. Klemm, W. R. Thiel, B. Plietker, *Angew Chem. Int. Ed.*, 2014, **53**, 7074–7078.
21 K. Koh, J. E. Seo, J. H. Lee, A. Goswami, C. W. Yoon and T. Asefa, *J Mater. Chem. A*, 2014, **2**, 20444–20449.
22 M. Yurderi, A. Bulut, N. Caner, M. Celebi, M. Kaya and M. Zahmakiran, *Chem. Commun.*, 2015, **51**, 11417–11420.
23 Z. L. Wang, J. M. Yan, Y. Ping, H. L. Wang, W. T. Zheng and Q. Jiang, *Angew Chem. Int. Ed.*, 2013, **52**, 4406–4409.
24 L. Yang, W. Luo and G. Z. Cheng, *Int. J Hydrogen Energy*, 2016, **41**, 439–446.
25 I. Schmidt, K. Müller and W. Arlt, *Energy Fuels*, 2014, **28**, 6540−6544.
26 M. Hattori, H. Einag, T. Daio and M. Tsuji, *J Mater. Chem. A*, 2015, **3**, 4453–4461.
27 Y. L. Qin, J. Wang, F. Z. Meng, L. M. Wang and X. B. Zhang, *Chem. Commun.*, 2013, **49**, 10028–10030.
28 S. Wu, F. Yang, H. Wang, R. Chen, P. C. Sun and T. H. Chen, *Chem. Commun.*, 2015, **51**, 10887–10890.
29 Z. L. Wang, J. M. Yan, H. L. Wang, Y. Ping and Q. Jiang, *Sci. Rep.*, 2012, **2**, 598.
30 Z. L. Wang, J. M. Yan, Y. F. Zhang, Y. Ping, H. L. Wang and Q. Jiang, *Nanoscale*, 2014, **6**, 3073–3077.
31 A. Bulut, M. Yurderi, Y. Karatas, Z. Say, H. Kivrak, M. Kaya and M. Zahmakiran, *ACS Catal.*, 2015, **5**, 6099–6110.
32 J. Liu, L. X. Lan, R. Li, X. Y. Liu, C. Wu, *Int. J Hydrogen Energy*, 2016, **41**, 951–958.
33 Z. L. Wang, Y. Ping, J. M. Yan, H. L. Wang and Q. Jiang, *Int. J Hydrogen Energy*, 2014, **39**, 4850–4856.
34 Y. Ping, J. M. Yan, Z. L. Wang, H. L. Wang and Q. Jiang, *J Mater. Chem. A*, 2013, **1**, 12188–12191.
35 H. M. Dai, N. Cao, L. Yang, J. Su, W. Luo and G. Z. Cheng, *J Mater. Chem. A*, 2014, **2**, 11060–11064.
36 H. M. Dai, B. Q. Xia, L. Wen, C. Du, J. Su, W. Luo and G. Z. Cheng, *Appl. Catal. B: Environ.*, 2015, **165**, 57–62.
37 Q. G. Liu, X. F. Yang, Y. Q. Huang, S. T. Xu, X. Su, X. L. Pan, J. M. Xu, A. Q. Wang, C. H. Liang, X. K. Wang and T. Zhang, *Energy Environ. Sci.*, 2015, **8**, 3204–3207.
38 C. González-Arellano, A. Corma, M. Iglesias and F. Sánchez, *Adv. Synth. Catal.*, 2004, **346**, 1758–1764.
39 C. González-Arellano, A. Corma, M. Iglesias and F. Sánchez, *Eur. J Inorg. Chem.*, 2008, **7**, 1107–1115.
40 Y. Himeda, *Green. Chem.*, 2009, **11**, 2018–2022.
41 D. Y. Zhao, J. Feng, Q. Huo, N. Melosh, G. H. Fredrickson, B. F. Chmelka, G. M. Whitesides and G. D. Stucky, *Science*, 1998, **279**, 548–552.
42 T. Yuan, H. F. Gong, K. Kailasam, Y. X. Zhao, A. Thomas, J. J. Zhu, *J. Catal.*, 2015, **326**, 38–42.
43 Xiao P, Zhao YX, Wang T, Zhan YY, Wang HH, Li JL, A. Thomas and J. J. Zhu, *Chem. Eur. J*, 2014, **20**, 2872–2878.
44 S. Zhang, Ö. Metin, D. Su and S. Sun, *Angew. Chem., Int. Ed.*, 2013, **52**, 3681-3684.
45 M. Yurderi, A. Bulut, M. Zahmakiran and M. Kaya, *Appl. Catal. B: Environ.*, 2014, **160-161**, 514-524.
46 X. Zhou, Y. Huang, W. Xing, C. Liu, J. Liao and T. Lu, *Chem. Commun.*, 2008, 3540–3542.
47 N. Yi, H. Saltsburg and M. Flytzani-Stephanopoulos, *ChemSusChem*, 2013, **6**, 816 -819.
48 K. Tedsree, T. Li, S. Jones, C. W. A. Chan, K. M. K. Yu, P. A. J. Bagot, E. A. Marquis, G. D. W. Smith and S. C. E. Tsang, *Nat. Nanotechnol.*, 2011, **6**, 302-307.
49 L. Yang, X. Hua, J. Su, W. Luo, S. L. Chen and G. Z. Cheng, *Appl. Catal. B: Environ.*, 2015, **168–169**, 423–428.
50 K. Mandal, D. Bhattacharjee and S. Dasgupta, *Int. J Hydrogen Energy*, 2015, **40**, 4786–4793.
51 Y. Q. Jiang, X. L. Fan, X. Z. Xiao, T. Qin, L. T. Zhang, F. L. Jiang, M. Li, S. Q. Li, H. W. Ge and L. X. Chen, *J Mater. Chem. A*, 2016, **4**, 657–666.
52 J. Y. Su, L. Zhu and G. H. Chen, *Appl. Catal. B: Environ.*, 2016, **186**, 127–135.